Nonlinear observer of crystal-size distribution during batch crystallization

Toufik Bakir, Sami Othman, Gilles Fevotte, Hassan Hammouri

1
Université de Lyon, Lyon, F-69003, France; Université Lyon 1;
CNRS UMR 5007 LAGEP (Laboratoire d'Automatique et de GEnie des Procédés),
43 bd du 11 novembre, 69100 Villeurbanne, France
Tel +33 (0) 4 72 43 18 45 - Fax +33 (0) 4 72 43 16 99
http://www-lagep.univ-lyon1.fr/ http://www.univ-lyon1.fr http://www.cnrs.fr

Nonlinear observer of crystal size distribution during batch crystallization

Bakir T, Othman S, Fevotte G, Hammouri H.

LAGEP, UPRES-A CNRS Q 5007/ CPE Université Claude Bernard

Lyon 1, 43 bd du 11 Nov. 1918, 69622 Villeurbanne Cedex France.

Abstract

A high gain observer was designed to estimate the CSD (Crystal Size Distribution) in batch crystallization processes. The observer is based on the discretization of population balance equations describing the evolution of the CSD using finite difference method. Due to process impurities and other batch-to-batch variations, the kinetic parameters involved in the dynamic model of the crystallization, relating primary and secondary nucleation in particular, are subject to significant variations. In order to avoid any estimation divergence, an on-line parameter identification algorithm was added to the observer. Assuming that measurements of the nuclei particles are available, the observer is shown to provide a discretized reconstruction of the entire CSD which can be used for control purposes or process supervision.

Keywords: Crystallization processes, high gain observer, non linear identification, population balance equations, crystal size distribution, finite difference method.

Introduction

In batch crystallization as well as in most particulate processes, the CSD (Crystal Size Distribution) influences the quality of the final product. This is particularly important as one considers both application and end-use properties of the crystallized product. However, measuring or estimating the CSD is really difficult and remains an open field of research.

Several techniques for the measurement of solute concentration have been used in the past, together with off-line image analysis for the modelling of the time variation of CSD during batch solution crystallizations (e.g. by [1], [2], [3], [4], [5], [6]) However it is important to notice that no online CSD measurements or estimates were available when such modelling studies were published.

Indeed several sensing in situ technologies are actually available which are supposed to yield, at least partially, the CSD during crystallization processes. However, no sensor can really provide accurate measurements of the whole CSD and even the physical significance of the measured sizes turns out to be questionable. For example, it is well known that the in-situ FBRM® probe (Focussed Beam Reflected Measurement) does not yield real particle size measurements, but chord length distributions CLD. In order to address this problem, the aim of the present work is to design an on line observer to reconstruct the entire crystal size distribution using both population balance equations and in-situ, in-line partial measurements. For example, measuring the number of nuclei (i.e. the smallest stable crystals) could be performed using the FBRM probe (Lasentec, Metters-Toledo). Worlitschek [7] has investigated the possibility of restoring CSDs from CLD data using Constrained Least Squares Minimization (CLSM). Turbidimetry can also be used to provide quantitative information on the number of small particles in suspension ([8], [9], [10]). Such sensors could provide reasonable information for the monitoring of the generation of nuclei even if bigger crystals cannot always satisfactorily be measured (e.g. turbidimetry is not suitable for big particles). This is why the reconstruction of the entire CSD from the measurement of the number of nuclei particles would undeniably be a valuable result.

As far as such observer is based on Population Balance Equations (PBE) describing the time variations of the CSD, it is essential that the PBE capture the main dynamic features of the process to yield good estimates.

Actually, the crystallization rate (i.e. the rate of generation of new crystallized solid) mainly depends on two mechanisms: crystal nucleation and growth. With the assumption of invariant kinetics parameters, the control of such process has been explored ([11], [12], [13]) However, it is clear that the parameters of primary nucleation involved in modeling and control studies may present drifts due to significant irreproducibility during the cooling crystallization process. In other words primary nucleation “seems” to exhibit random features, which can be experimentally observed as batch-to-batch variability. Such variability is inherent to the highly non linear features of the crystallization mechanisms, and it is generally attributed to possible impurities in the load of the reactor, and to strong dependency of most basic crystallization phenomena on tiny differences in the operating conditions (e.g. presence of small residual crystals on the reactor wall at the beginning of the batch process). Moreover, from a more technical point of view, it is necessary to evaluate the robustness of the estimation process to parameter uncertainties. This is a second reason why the initial values of the nucleation parameters used by the state observer were set to be different from the values which were supposed to relate the “true” experimental nucleation kinetics.

The on-line identification of nucleation parameters was therefore necessary to avoid potential drifts of the observer. In order to deal with this difficulty, the available measurements can also be used to estimate the nucleation parameter(s) in question. In the following, it is shown that combining on-line parameter identification with high-gain CSD estimation allows to efficiently monitor the crystallization process.

The paper is organized as follows; first the batch crystallization model is briefly described in section 2. The principle of the discretization of the PBE (Population Balance Equations) involved is then exposed in section 3. In section 4, a method for the on-line identification of a

'sensitive' primary nucleation parameter is presented. Section 5 is devoted to the observer synthesis and the estimation technique is validated through simulation in section 6.

Model development

The population balance approach applied to batch crystallizer yields the following partial differential equation (PDE):

$$\frac{\partial n(x,t)}{\partial t} + G(t)\frac{\partial n(x,t)}{\partial x} = 0 \qquad (1)$$

$n(x,t)$ is a number population density function. It represents the number of crystals of size x per unit volume of suspension and per unit of size. In model (1), only nucleation and growth will be considered, agglomeration and breakage are not taken into account. The growth kinetic $G(t)$ is assumed to be size independent. The solute concentration balance describing the mass transfer from the liquid to the solid phase is:

$$\frac{dV_t(t)C(t)}{dt} + \frac{dV_T(t)C_S(t)}{dt} = 0 \qquad (2)$$

$C(t)$ represents the solute concentration, $V_T(t)$ is the suspension volume, variations of this volume, due to solute mass transfer can be neglected. $C_S(t)$ being the solid concentration, it is easily deduced from the crystal size distribution (CSD) :

$$C_S(t) = \frac{K_v \rho_s}{M_s}\int_{x^*}^{x^\infty} x^3 n(x,t)dx \qquad (3)$$

where K_v is a shape factor (e.g. for spherical particles $K_v = \frac{\pi}{6}$), M_s is the molecular weight of the crystallized solid of density ρ_s, and $V_t(t)$ is the solution volume (i.e. volume of the continuous phase), which is calculated from the following expression :

$$V_t = V_T(1 - \frac{M_S}{\rho_S}C_S) \qquad (4)$$

The crystallizer temperature is given by the energy balance around the cooling jacket wall :

$$\sum_{i=1}^{3} Cp_i\, n_i \frac{dT_{cr}}{dt} = -\Delta H_c\, V_T \frac{dC_S}{dt} - UA_c (T_{cr} - T_j) \quad (5)$$

where Cp_i and n_i represent respectively the molar heat capacities and number of moles of the different components in the crystallizer. T_{cr} and T_j are respectively the crystallizer and jacket temperatures. ΔH_c is the crystallization enthalpy. U and A_c are respectively the overall heat transfer coefficient and contact surface of the jacket wall. The solubility, which refers to the solute concentration under saturated conditions, is assumed to obey Van't Hoff equation:

$$C_{sat}(T_{cr}) = A e^{-\left(\frac{\Delta H}{RT_{cr}}\right)} \quad (6)$$

The absolute supersaturation $(C - C_{sat})$ is the driving force of the crystallization process. The overall growth rate, including possible diffusive limitations, is assumed to be represented by the following model. In the literature, values of exponent g are generally assumed to lie between 1 and 2 [15]:

$$G(t) = K_c \frac{M_s}{2\rho_s} \eta (C - C_{sat})^g \quad (7)$$

Where K_c represents the kinetic growth rate coefficient, η represents the effectiveness factor which is the solution of the following equation:

$$\left[\frac{K_c}{K_d}(C - C_{sat})^{g-1}\right]\eta + \eta^{(1/g)} + 1 = 0 \quad (8)$$

According to [14], η relates the actual mass flux of solid integrated in the crystal structure to the maximum theoretical flux that would be integrated in the absence of diffusive limitation. For very small particles, η is usually close to 1, which means that the mass transfer resistance, due to the diffusion of solute from the bulk to the crystal surface, is negligible for the smaller crystals.

K_d represents the mass transfer coefficient through diffusion. Analytical solution of eq. (8) are available if g is equal to 1 or 2, a numerical solution can be considered in the other cases.

The nucleation rate B is the result of two competitive nucleation mechanisms. Primary nucleation B_1 takes place in the absence of any crystal in the solution [15]:

$$B_1 = a_{N1} e^{-\left(\frac{b_{N1}}{\ln^2(\frac{C}{C_{sat}})} \right)} \quad (9)$$

Where $\beta = \frac{C}{C_{sat}}$ is referred to as the degree of supersaturation.

Secondary nucleation B_2, which may occur at lower supersaturation level, is favored by the presence of solid in suspension (i.e. added in the crystallizer through seeding or generated through primary nucleation):

$$B_2 = a_{N2} M_T^i (C - C_{sat})^j \quad (10)$$

The primary nucleation parameter a_{N1} requires to be identified on-line, a_{N2} and b_{N1} are assumed constant and M_T is the overall mass of solid in suspension. The boundary condition for equation (1) is usually set as follows [16]:

$$n(x^*, t) = \frac{B_N(x^*)}{G(x^*)} = \frac{B}{G} \quad (11)$$

Where, according to free energy considerations, only crystal nuclei of critical size x^* are assumed to grow. (i.e. for $x < x^*$, the particle will dissolve).

Secondary nucleation clearly appears to be less “explosive” than primary nucleation and it is known to take place at lower supersaturation values. In other words, the limit curve of metastable zone for secondary nucleation is closer to the solubility curve than the limit curve of metastable zone for primary nucleation [15]. Actually, it is usually assumed that secondary nucleation dominates nucleation phenomena in most industrial crystallization processes. As already mentioned, seeding the crystallizer yields secondary nucleation, provided that the

supersaturation level is sufficient. The mass of seed should yet be sufficient to allow significant consumption of solute through crystal growth and, consequently, avoid undesirable primary heterogeneous nucleation burst. Therefore, satisfactory seeding conditions are expected to lead to both moderate increase in the particle number and supersaturation decrease. In the following, unseeded crystallization operations (i.e. primary nucleation takes place) are referred to as "case 1" while seeded crystallizations are referred to as "case 2".

Discretization of the PBE "Population Balance Equation"

Many discretization methods were applied to the PBEs (see e.g. [17] and [18]). Finite difference methods which are widely developed in numerical analysis and collocation methods supported by [19] were both applied during the present study. The discretization of the crystallization PDE using the first method is rather well developed. Interestingly, finite difference method fits exactly the observer structure. Indeed, the state matrix involved exhibits tri-diagonal form. Moreover, the method is consistent with the physical behavior of the system. Meanwhile, collocation techniques are based upon polynomial approximations correlating states from a mathematical point of view, rather than from the physical point of view. The system resulting from the discretization finally turns out to be:

$$\begin{cases} \dot{n}_x = \alpha(t)\, A\, n_x \\ y = C\, n_x \end{cases} \qquad with: \quad \alpha(t) = \frac{G(t)}{\Delta x} \tag{12}$$

$$n_x = \begin{bmatrix} n_{x_1} \\ n_{x_2} \\ n_{x_3} \\ \vdots \\ n_{x_{N-1}} \\ n_{x_N} \end{bmatrix}, \; A = \begin{bmatrix} 1 & -1 & 0 & \cdots & 0 \\ \frac{1}{2} & 0 & -\frac{1}{2} & \cdots & 0 \\ 0 & \ddots & \ddots & \ddots & \vdots \\ \vdots & \ddots & \frac{1}{2} & 0 & -\frac{1}{2} \\ 0 & \cdots & 0 & 0 & 0 \end{bmatrix}$$

$$C = \begin{bmatrix} 1 & 0 & \cdots & \cdots & \cdots 0 \end{bmatrix},$$

With $n_x \in \Re^N \times \Re^N$ and $C \in \Re^N$. Equations (11-12) assume that the number $n_{x_1}(t)$ of particles with minimum size that can be measured represents the number of nuclei $n(x^*,t)$. Such assumption is valid if the time required by a given nucleus to grow until the minimum detectable size is supposed to be negligible.

The moment's equations of the CSD are defined by :

$$\mu_i = \int_{x^*}^{x^\infty} x^i n(x,t)dx \qquad i = 0,1,2,3 \qquad (13)$$

The computation of the moments allows evaluating overall parameters characterizing the CSD like the number mean size L_{pop} and the variation coefficient VC_{pop} which are calculated as follows:

$$L_{pop} = \frac{\mu_1}{\mu_0} \qquad (14)$$

$$VC_{pop} = \sqrt{\frac{\mu_0 \mu_2}{\mu_1^2} - 1} \qquad (15)$$

Identification of primary nucleation parameter a_{N1}

Mechanistic modelling of primary homogeneous nucleation was reported by many authors, and complex models were proposed for both parameters a_{N1} and b_{N1}. However, industrial and laboratory practice clearly show that the reported nucleation models cannot be considered as fully predictive. A good illustration of this problem lies in the fact that, despite reproducible operating conditions, it is very frequent to observe batch-to-batch varying nucleation temperatures related to irreproducible occurrence of the primary nucleation. The resulting variations of nucleation supersaturation, conjugated with the highly non linear features of the nucleation kinetics induce dramatic batch-to-batch changes of the particle number. As far as CSD modelling and estimation is concerned, it would therefore be illusory

to rely on constant nucleation parameter values. In the following approach, it is assumed that a_{N1} is a highly uncertain parameter while b_{N1} is assumed constant, with possible differences with respect to the simulated "true" value. In order to estimate the time variations of the CSD, a state observer was designed assuming that measurements of the number of the initial particles (i.e., the nuclei) are performed. In order to strengthen the estimation scheme, parameter a_{N1} was also estimated. A Levenberg-Marquardt algorithm was used to perform such identification, it is based on the minimization of the following quadratic error criterion:

$$J(\theta) = \sum_{i=1}^{N} (y_m(t_i) - y(t_i, \theta))^2 = \sum_{i=1}^{N} (e_i(\theta)).^2 \qquad (16)$$

The identification is performed on adequate sliding horizon of points. Measurement and pseudo-measurements being available, the estimation of the crystal size distributions and the calculation of the moments resulting from this estimation can be performed. It is worth noting that, in contradiction with CSD measurements, solute concentration measurements are currently available in-line ([20], [21]). For example ATR FTIR *in situ* solute concentration measurements were successfully performed for several model crystallization systems. Using such technique, our group has reported relative uncertainties of the order of 1-2%, in the case of various organic batch crystallization operations (see e.g. [20], [26], [27]). These latter measurements can be used to compute the time variations of supersaturation and, therefore, the nucleation and growth kinetics leading to the number of generated nuclei, according to eq.(11). The estimated values of $n(x^*, t)$ are then considered as pseudo-measurements which can be updated using any infrequent and/or off-line CSD measurement, allowing variations of parameter a_{N1} to be identified. Such identification of the nucleation kinetic rate B_1 improves the observer convergence.

It is clear that, given the structure of the primary nucleation model, the identification of both parameters a_{N1} and b_{N1} is impossible from the measurements which are assumed to be

available. However preliminary simulations have clearly shown that for any reasonably uncertain initial value of b_{N1}, the observer yields appropriate value of a_{N1} such that the reconstructed CSD is satisfactory. For example, in the following b_{N1} was assumed to be equal to 0.69 (see Table 1) which led to the time variations of displayed in Figure 2. Setting b_{N1} to 0.9 obviously yielded different variations of parameter a_{N1}, with a maximum of 0.6 10^{12} nb.m^{-3}.s^{-1}. However, in both cases, the two estimated pairs (a_{N1}, b_{N1}) produced really similar CSD profiles.

High gain observer synthesis

In the case of single output systems, the high gain observer is dedicated to the uniformly observable systems class of the following form:

$$\begin{cases} \dot{z} = f(z) + \sum_{i=1}^{P} u_i g_i(z) \\ y = h(x) \end{cases} \qquad (17)$$

where $z \in \Re^N$, $y \in \Re$, $u \in \Re^P$

System (17) is said to be uniformly observable if for any two initial states $z \neq \bar{z}$ and every admissible inputs defined on any [0,T], there exists t$\in$[0,T] such that $y(z,u,t) \neq \bar{y}(\bar{z},u,t)$, where $y(z,u,t)$ is the output associated to the initial state z and the input u. This means that the observability of the system is not affected by the variation of the input u in the interval of observation [0, T].

Here, system (17) takes the particular form of system (12) which is clearly observable due to its triangular form. Indeed, in this particular case, the structure of the different differential equations (matrix A) shows that, on the observation interval, a given output trajectory implies

a unique solution of the set of the other crystal classes. Such observability can be proved using the well known Kalman criterion: rank[(C, CA, …, CA^{N-1})]=N.

The canonical form may be used to construct an exponential observer for system (12) under the following technical assumption:

$\exists \gamma, \xi \quad with \quad 0 < \gamma \le \xi, \forall t \le 0 : \gamma \le \alpha(t) \le \xi$ for some constant γ and ξ.

As α(t) represents the growth kinetic which is positive and bounded, this assumption is not restrictive in the case of crystallization processes.

In the case of continuous measurements, a candidate exponential observer for the system is given by [22] and [23]:

$$\dot{\hat{z}}(t) = \alpha(t) A \hat{z}(t) - \alpha(t) S_\theta^{-1} C^T (C \hat{z}(t) - y(t)) \tag{18}$$

where S is symmetric positive definite matrix given by the following equation:

$$\dot{S}_\theta(t) = -\theta S_\theta(t) - A^T S_\theta(t) - S_\theta(t) A + C^T C \tag{19}$$

If $\alpha(t)$ is negative for any time t>0, the sign of the correction term should be changed:

$$\dot{\hat{z}}(t) = \alpha(t) A \hat{z}(t) + \alpha(t) S_\theta^{-1} C^T (C \hat{z}(t) - y(t)) \tag{20}$$

Case 2 requires to apply the previous model when seeding is performed. Here the discretization is based upon about 50 samples. This number was chosen to allow satisfactory accuracy of the model representation. The same number of samples was used in the observer synthesis, while in case 1, *N* was set to 100 so as to improve the model accuracy. Such a number is not harmful to the observer computation time, and could be reduced to a quarter $N_{observer} = 25$. The latter simplification allows one to significantly reduce the observer variables, and consequently allows saving significant computation time. The model-predicted variables and the corresponding estimates will be compared in the next section.

For case 1 (unseeded solution), matrix A in equation (12) is replaced by:

$$A = \begin{bmatrix} \frac{1}{ratio} & \frac{-1}{ratio} & 0 & \cdots & 0 \\ \frac{1}{2ratio} & 0 & \frac{-1}{2ratio} & \cdots & 0 \\ 0 & \ddots & \ddots & \ddots & \vdots \\ \vdots & \ddots & \frac{1}{2ratio} & 0 & \frac{-1}{2ratio} \\ 0 & \cdots & 0 & 0 & 0 \end{bmatrix}$$

with: $$ratio = \frac{N}{N_{observer}}$$

In other words: $$A_1 = \frac{A}{ratio}$$

In order to make use of the previous observer structure, we consider the following change of variables:

$$\alpha_1(t) = \frac{\alpha(t)}{ratio} = \frac{G(t)}{\Delta x \; ratio} \tag{21}$$

The new system is given by:

$$\begin{cases} \dot{n}_{x_{observer}}(t) = \alpha_1(t) A n_{x_{observer}}(t) \\ y(t) = C n_{x_{observer}}(t) \end{cases} \tag{22}$$

Despite the change of coordinates the structure remains unchanged. Reducing the number of variable in the gain matrix S allows saving integration computation time. The new number of S components being $\frac{(1+N_1)(N_1-1)}{2}$.

Another alternative is to use the following diffeomorphism ϕ :

$$\begin{aligned} \phi : \Re^N &\to \Re^N \\ z &\to \left[h, L_f(h), \cdots, L_f^{N-1}(h)\right] \end{aligned}$$

Such diffeomorphism transforms system (12) into the observable canonical form with:

$$A_2 = \begin{bmatrix} 0 & 1 & \cdots & 0 \\ 0 & 0 & \ddots & \vdots \\ \vdots & \vdots & \ddots & 1 \\ 0 & 0 & \cdots & 0 \end{bmatrix},\ C_2 = \begin{bmatrix} 1 & 0 & \cdots & 0 \end{bmatrix}$$

The resulting observer exhibits the following form:

$$\dot{\hat{z}} = \alpha(t) A \hat{z} - \alpha(t) \left(\frac{\partial \phi}{\partial z}(\hat{z}, t) \right)^{-1} S_\theta^{-1} C_2^T (C_2 \hat{z} - y) \tag{23}$$

Where S_θ is given by the Lyapunov equation:

$$\theta S_\theta + A_2^T S_\theta + S_\theta A_2 = C_2^T C_2 \tag{24}$$

The terms of matrix $S_\theta = \left[S_\theta(l,k) \right]_{1 \le l,k \le N}$ are given by:

$$S_\theta(l,k) = \frac{(-1)^{l+k} D_{l+k-2}^{k-1}}{\theta^{l+k-1}} \tag{25}$$

With: $$D_n^k = \frac{n!}{(n-k)!k!} \tag{26}$$

In the present case, the calculation of ϕ is straightforward because matrix *A* is constant. The result is given by the following equation:

$$\phi = \phi_1 z \tag{27}$$

With: $$\phi_1 = \left[C, CA, \cdots, CA^{N-1} \right] \tag{28}$$

And thus:

$$\left(\frac{\partial \phi}{\partial z}(\hat{z}, t) \right)^{-1} = \left[C, CA, \cdots, CA^{N-1} \right] \tag{29}$$

Simulation results and discussion

Simulation conditions

The parameters used to simulate an industrial batch crystallization process were taken from the in depth investigation of the crystallization of adipic acid in water reported by Marchal

[24]. Primary homogenous nucleation models were also taken from [25]. The cooling fluid in the jacket was assumed to be brine at $0\,^{\circ}C$. Table 1 summarizes both the kinetic and operating parameter values which were used during the simulation.

Simulation results and discussion, case 1

Figure 1 displays the concentration diagram of a typical simulated unseeded batch crystallization process. The model simulated operating conditions are the following:

- The initial undersaturated adipic acid solution is kept to 50 °C (323 K). The initial solute concentration is 1550 mol/m^3 while the corresponding solubility is about 1500 mol/m^3.
- Cooling is assumed through temperature controlled brine initially kept at 320 K (i.e. the initial temperature difference between the jacket and the solution is 3 °C). The set point trajectory for the cooling brine tracks a constant rate of -1 °C/min until the final crystallizer temperature is reached (280 K).

Stirring effects are not explicitly taken into account in the crystallization model even through it is well-known that nucleation phenomena are likely to strongly depend on the stirring power. However, it is assumed that such effects are indirectly represented through possible variations of the nucleation kinetic parameters.

The width of metastable zone appears to be rather large while the residual supersaturation following the initial nucleation and growth process remains very low. Indeed, Fig. 1 shows that due to primary nucleation and growth of the newly generated particles, the solute concentration starts to decrease at about 313 K. the corresponding solubility is about 1020 mol/m^3 and the initial supersaturation is therefore C-C_{sat}=1550-1020=530 mol/m^3 . This latter point, together with the fast return to solubility after primary nucleation indicates that the simulated growth rate is sufficient to allow fast consumption of the solute during the cooling process after nucleation. This experimental behavior is indeed observed during the industrial

crystallization of adipic acid in water. Consequently, due to the low supersaturation values, reduced secondary nucleation is expected during the continuation of the batch process.

Identification of parameter a_{N1} is shown in figure 2. Despite the simulation of a significant initial uncertainty, the convergence appears to be very fast at the onset of primary nucleation (i.e. after about 140 s which corresponds to T=312 K the nucleation process is observed). The identification then appears to be really stable, accurate and efficient in tracking slight temperature variations of parameter a_{N1}. However, after about 400 s, the estimation process loses its efficiency, which is neither surprising nor detrimental since, due to negligible supersaturation level, the nucleation process is almost terminated.

Figure 3 display the time variations of the number of nuclei which are assumed to be imperfectly measured. A noise (gaussian noise with variance of about 0,38) was added to the "real" simulated data of the number of generated nuclei (i.e. as outlined above, crystals contained in the smallest size class.) Again, the convergence of the estimated number of small particles appears to be satisfactory.

As examples of the estimation of particle numbers in the different size classes, Figures 4 and 5 show a comparison between the evolutions of the numbers of particles in the 9th and 57th model classes, respectively. These two classes of size correspond to $18\,\mu$m and $104\,\mu$m, respectively. The classes in Figs. 4 and 5 were arbitrarily selected to illustrate the convergence and the performance of the observer. The whole range of other simulated classes yielded similar results. In figure 4, the estimation of the number of small particles appears to be less stable than for bigger crystals in Figure 5. This is simply due to the fact that big particles do not disappear through growth at the end of the batch process while, due to the

cancellation of primary nucleation when supersaturation tends towards zero, the growth of smaller particles make them vanish in the size distribution.

Even though they provide reduced information about the CSD, the moments of the size distribution can be considered as representative of the accuracy of the reconstruction of the whole size distribution. From this point of view, Figure 6 represents the third moment which is required to compute the weight average particle size. Figure 7 displays the number average crystal size (i.e., the ratio $L_{mean} = \frac{\mu_1}{\mu_0}$) It appears that, except before the occurrence of significant primary nucleation (i.e., before the time when it is meaningless to estimate the particle sizes), the average size and the moments are well estimated by the high gain observer. Finally, a presentation of the simulated CSD, compared with the reconstructed CSD obtained with reduced number of size classes, is given in Figures 8, 9. As expected from the previous comparisons, the fit between the two plots is satisfactory.

Simulation results and discussion, case 2

Seeded crystallizations (i.e. case 2) are usually performed in order to circumvent the effects of the primary homogeneous nucleation burst, and therefore reduce the detrimental effect of too large a number of initial particles on the final CSD. Simulating such operating mode requires the knowledge of both the number and size distribution of the seed particles. In the following, the mass of seed is set to 5% of the overall expected mass of crystallized product, and its average particle size is of the order of 20 μm. In order to evaluate the convergence of the observer, a 10% uncertainty was added to every class of the initial seed CSD (i.e., to the simulated "real" seed CSD) and introduced as initial CSD estimate. Figure 10 shows the difference between the "actual" seed CSD and the initial guess used by the observer.

Seeding batch crystallizers results in lower initial supersaturation levels, due to the growth of seeds. Consequently, the variation of the CSD during seeded crystallizations (case 2) is slower than during unseeded operations. This is the reason why satisfactory operation of the state observer during seeded operations was found to require fewer measurements than during "case 1" situations. Figure 11 demonstrates the very fast convergence of the estimation algorithm to reconstruct the time variations of the number of nuclei particles during the seeded process.

Finally, Fig. 12 shows a rather satisfactory comparison between both estimated and simulated number average particle sizes L_{mean}. At the beginning of the crystallization, as expected, the average size is overestimated, due to the initial underestimation of the particle number (i.e. less particles from bigger size classes). At the end of the batch process, the relative uncertainty of the estimates is of the order of 5%.

Conclusions

Actually, the more sophisticated commercially available particle analyzers are unable to provide accurate and reliable measurements of the "real" particle size distribution during crystallization processes. For both theoretical and numerical reasons, even for suspensions exhibiting ideal properties (such as spherical particle shapes and monomodal distributions) extracting indicative CSD from sensors raw data remains an open problem. In order to address this important difficulty, one can expect powerful state estimation techniques to allow the reconstruction of CSD from partial measurements of the size distribution.

An observation approach based on the design of a high gain observer is presented here, which is shown to be efficient in simulation. The proposed state observer assumes in-line measurements of the number of nuclei particles (i.e. of the smallest stable crystals in

suspension). Such requirement, which indeed is rather demanding, is not that unrealistic due to the significant progresses accomplished in the field of particle sensing technologies together with the possibility of using physical or statistical models to extract dependable nucleation data from imperfect measurements. The infinite dimensional system describing the time variations of the particle sizes was discretized, allowing a state formulation of the population balance equations. Even though it is theoretically possible, the estimation of huge a number of variables (the size classes) is numerically difficult to implement. This is why a reduction of the order of the state observer was performed. Primary nucleation was assumed to be the main crystallization mechanism governing the CSD and particular attention was paid to the potential batch-to-batch variations of the pre-exponential parameter a_{N1} involved in the primary nucleation rate model. In order to increase the robustness of the observer, the batch-to-batch and time variations of a_{N1} were identified using a Levenberg-Marquardt algorithm. Through simulation studies, it is shown that the whole state observation strategy is really efficient in reconstructing the time evolutions of the CSD, as far as significant variations of the particle size take place (i.e. when unegligible supersaturation is generated as the driving force of crystal growth).

References

[1] Braatz RD, Hasebe S. Particle size and shape control in crystallization processes. AIChE symp series. 2002;326:307-327.

[2] Feng L, Berglund KA. "ATR-FTIR" for determining optimal cooling curves for batch crystallization of Succinic Acid. Crystal Growth and Design. 2002;5:449-452.

[3] Puel F, Févotte G, Klein JP. Simulation and analysis of industrial crystallization processes through multidimensional population balance equations. Part 1: a resolution algorithm based on the method of classes. Chemical Engineering Science. 2003;58:3715-3727.

[4] Rawlings JP, Miller SM, Witkowski WR. Model identification and control of solution crystallization process : a review. Ind. Eng. Chem. Res. 1993;32:1275-1296.

[5] Rohani S. Crystallization kinetics, modeling and control: a review. Trends in chemical engineering. 1998;5:173-193.

[6] Worlitschek J, Mazzotti M. Model-based optimization of patricle size distribution in batch-cooling crystallization of Paracetamol. Crystal Growth and Design.2004;4:891-903.

[7] Worlischek J. Monitoring, modeling and optimization of batch cooling crystallization. PhD dissertation, ETH n° 15189, Zurich, Germany. 2003.

[8] Zollars, Richard L. Turbidimetric method for on-line determination of latex particle number and particle size distribution. Journal of Colloid and Interface Science (1980), 74(1), 163-72.

[9] Herri, J. M.; Gruy, F.; Pic, J. S.; Cournil, M.; Cingotti, B.; Sinquin, A. Interest of in situ turbidimetry for the characterization of methane hydrate crystallization: application to the study of kinetic inhibitors. Chemical Engineering Science (1999), 54(12), 1849-1858.

[10] Moscosa-Santillan, M.; Bals, O.; Fauduet, H.; Porte, C.; Delacroix, A. Study of batch crystallization and determination of an alternative temperature-time profile by on-line

turbidity analysis - application to glycine crystallization. Chemical Engineering Science (2000), 55(18), 3759-3770.

[11] Jones AG. Optimal operation of a batch cooling crystallizer. Chemical Engineering Science. 1974;29:1075-1087.

[12] Rohani S.Self-tuning control of crystal size distribution in a cooling batch crystallizer. Chemical Engineering Science. 1990;45:3457-3466.

[13] Zoltan KN, Richard DB. Open loop and closed-loop robust optimal control of batch processes using distributional and worst case analysis. Journal of Process Control. 2004;411-422.

[14] Garside J. The concept of effectiveness factors in crystal growth. Chem. Engng. Sci. 1971);26: 1425-1431.

[15] Mersmann A. Crystallization Technology Handbook, 2nd Ed. Mersmann. New York., Marcel Dekker. 2002.

[16] Ramkrishna, D. (2000). Population balances. Theory and applications to particulate systems in engineering. New York: Academic Press.

[17] Kumar, S., Ramkrishna D. On the solution of population balance equations by discretization-III.Nucleation, grouth and aggregation of particles. Chemical Engineering Science. 1997;52:4659-4679.

[18] Liu Y, Cameron IT. A new wavelet-based adaptive method for solving population balance equations. Powder Technology. 2003;181-188.

[19] Villadsen JV, Stewart WE.Solution of boundary-value problems by orthogonal collocation. Chemical Engineering Science. 1966;22:1483-1501.

[20] Fevotte G. "New perspectives for the on-line monitoring of pharmaceutical crystallization processes using in situ infrared spectroscopy." International Journal of Pharmaceutics. 2002:**241**(2): 263-278.

[21] Yu L. X., Lionberger R. A., Raw A. S., D'Costa R., Wu H., Hussain A. S. "Applications of process analytical technology to crystallization processes." Advanced Drug Delivery Reviews. 2004 :**56**(3): 349-369.

[22] Farza M, Hammouri H, Othman S, Busawon K. Nonlinear observer for parameter estimation in bioprocesses. Chemical Engineering Science. 1997;52:4251-4267.

[23] Gauthier JP. Hammouri H, Othman S. A simple observer for non linear systems Application to bioreactors. IEEE Trans. Automat. Control. 1992;37:875-880.

[24] Marchal P.Génie de la cristallisation: application à l'acide adipique. Thèse, Institut National Polytechnique de Lorraine, Nancy.1989.

[25] Mersmann A, Braun B, Löfflmann M. Prediction of crystallization coefficients of the population balance. Chemical Engineering Science. 2000;57:4267-4275.

[26] Lewiner, F., Klein, J.P., Puel, F., Fevotte, G. (2001). “on-line ATR FTIR measurement of supersaturation during solution crystallization processes. Calibration and applications on three solute/solvent systems.” Chemical Engneering Science 56(6): 2069-2084.

[27] Oullion, M.P., Fevotte, G., Klein, J.P., Righini, S., Carvin, P. (2005). “Monitoring and modelling batch crystallization of a food ingredient” 16th International Symposium of Industrial Crystallization ISIC’16, Dresde, 11-14 sept.

Table 1. Parameters used for the simulation of the crystallization phenomena, after Marchal [22]

Parameter	Definition	Unit	Value
a_{N1}	Pre-exponential primary homogeneous nucleation parameter	$nb.m^{-3}.s^{-1}$	Computed from [15, 24]
b_{N1}	Exponential primary homogeneous nucleation parameter	No dimension	0.69
a_{N2}	Secondary nucleation parameter	$nb.m^{3(I+j-1)}.mol^{-i-j}.s^{-1}$	1440
K_c	Growth constant	$mol^{(1-g)}.m^{(3g-2)}.s^{-1}$	$1.57\ 10^{-2}$
i	Exponent	No dimension	1.968
j	Exponent	No dimension	1
g	Exponent	No dimension	2
M_s	Molar mass of the solute	$Kg.mol^{-1}$	$146.14\ 10^{-3}$
ρ_s	Density of the solute	$Kg.m^{-3}$	1360
K_v	Crystal shape factor	No dimension	π/6
Cp_1	Solute molar heat capacity	$J.K^{-1}.mol^{-1}$	3.72
Cp_2	Molar heat capacity of the solid	$J.K^{-1}.mol^{-1}$	7.44
Cp_3	Molar heat capacity of water	$J.K^{-1}.mol^{-1}$	75.33
ΔH_c	Crystallization enthalpy	$J.mol^{-1}$	-48000
U	Overall heat transfer coefficient through the jacket	$W.m^{-2}.K^{-1}$	1000
A_c	Contact surface of the jacket	m^2	$2.2\ 10^{-2}$

Figures Captions

Figure 1: Solubility curve (dashed line) and simulation of the concentration profile (solid line) during unseeded batch cooling crystallization of adipic acid

Figure 2: Simulated variations of the primary nucleation parameter a_{N1} (continuous line) and estimates using Levenberg-Marquardt Algorithm (Dashed line)

Figure 3: Simulated measurement of the number of nuclei (continuous line) and estimates (Dashed line) during unseeded batch cooling crystallization.

Figure 4: Simulation (solid line) and reconstructed time variations (Dashed line) of the 9th size class (18 μm) of the model (i.e. the 3rd size class of the state observer) during unseeded batch cooling crystallization.

Figure 5: Simulation (solid line) and reconstructed time variations (Dashed line) of the 57th size class (104 μm) of the model (i.e. the 15th size class of the state observer) during unseeded batch cooling crystallization.

Figure 6: Simulation (solid line) and reconstructed time variations (Dashed line) of the third moment of the size distribution during unseeded batch cooling crystallization.

Figure 7: Simulation (solid line) and reconstructed time variations (Dashed line) of the number average particle size during unseeded batch cooling crystallization.

Figure 8: Simulation of the time variations of the CSD during unseeded batch cooling crystallization of adipic acid.

Figure 9: Estimation of the time variations of the CSD during unseeded batch cooling crystallization of adipic acid.

Figure 10: (dashed line) Initial observer CSD (A 10% uncertainty was added to the simulated seed CSD) and (solid line) simulated seed CSD during “case 2” batch cooling crystallization.

Figure 11: Simulated measurement of the number of nuclei (continuous line) and estimates (Dashed line) during seeded batch cooling crystallization.

Figure 12: Simulation (solid line) and reconstructed time variations (Dashed line) of the number average particle size during seeded batch cooling crystallization.

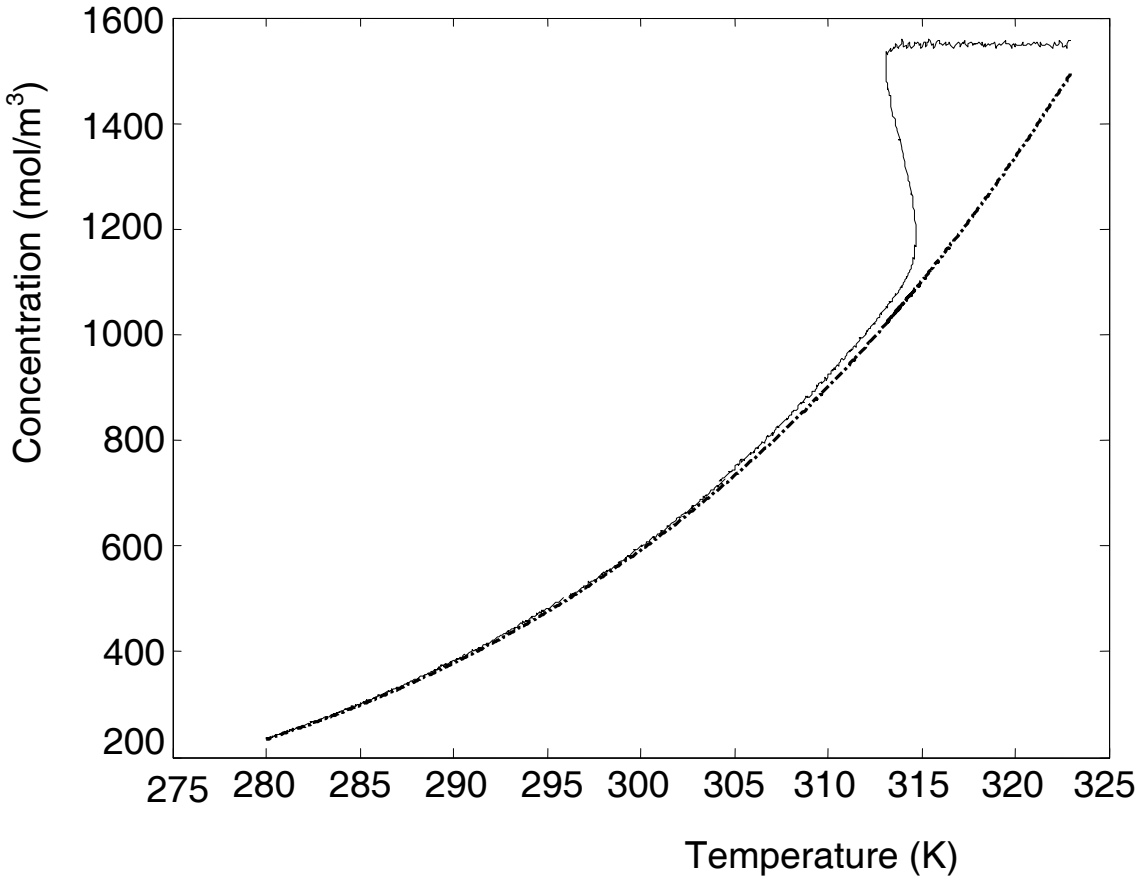

Figure 1: Solubility curve (dashed line) and simulation of the concentration profile (solid line) during unseeded batch cooling crystallization of adipic acid

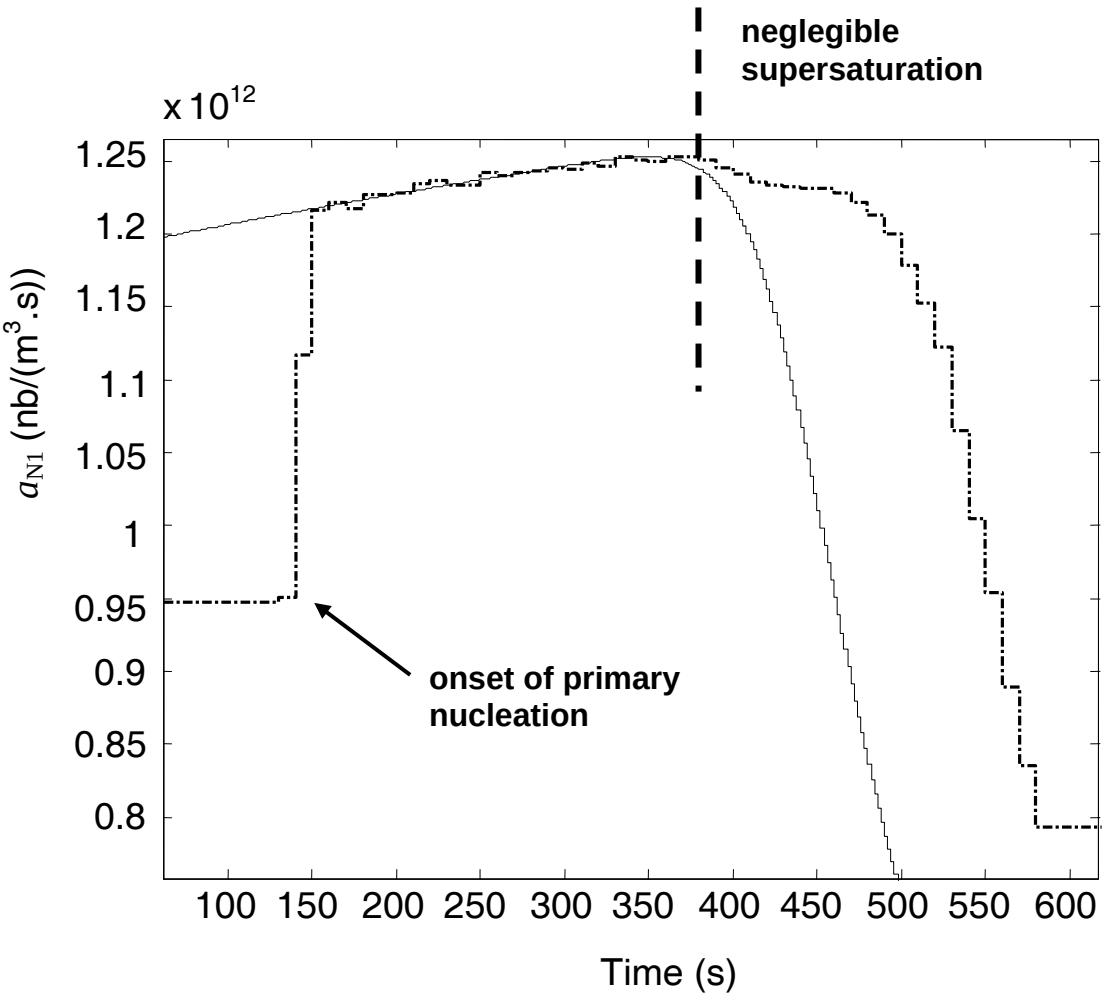

Figure 2: Simulated variations of the primary nucleation parameter a_{N1} (continuous line) and estimates using Levenberg-Marquardt Algorithm (Dashed line)

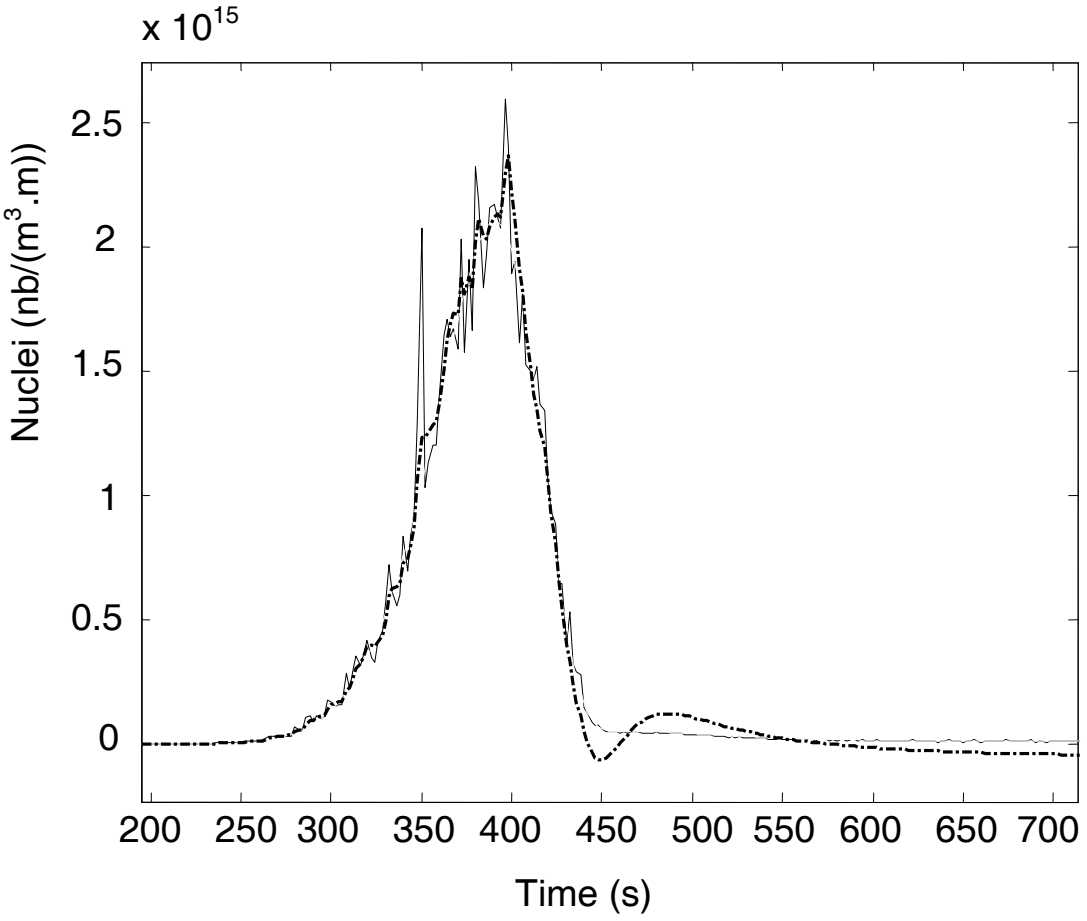

Figure 3: Simulated measurement of the number of nuclei (continuous line) and estimates (Dashed line) during unseeded batch cooling crystallization

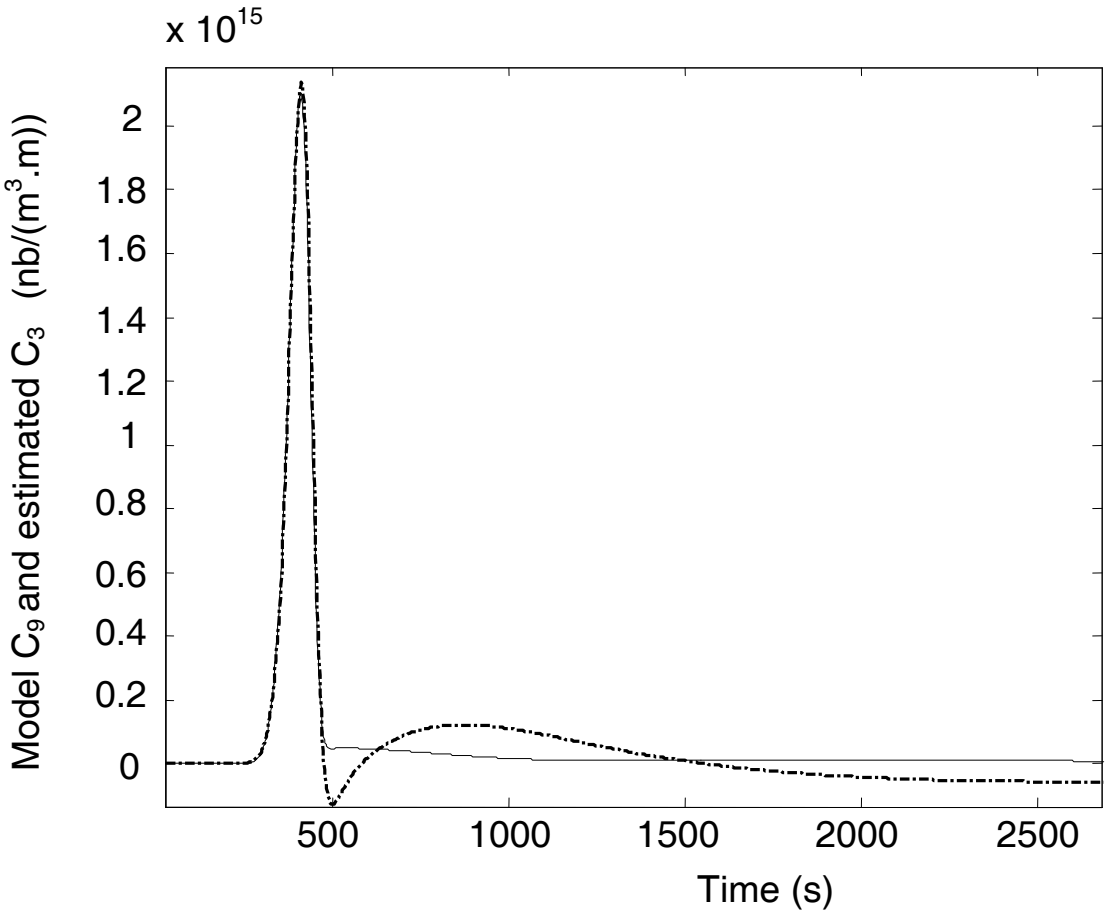

Figure 4: Simulation (solid line) and reconstructed time variations (Dashed line) of the 9th size class (18 μ m) of the model (i.e. the 3rd size class of the state observer) during unseeded batch cooling crystallization.

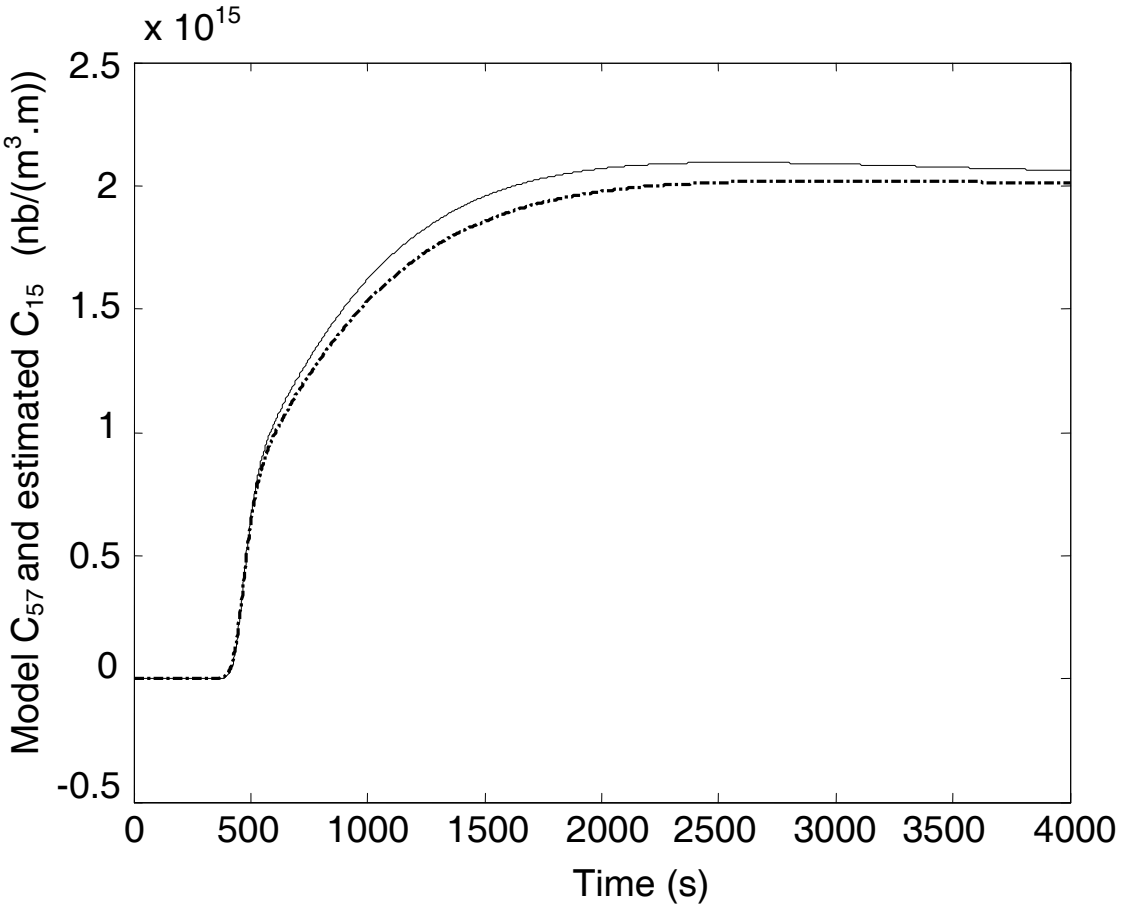

Figure 5: Simulation (solid line) and reconstructed time variations (Dashed line) of the 57th size class (104 μm) of the model (i.e. the 15th size class of the state observer) during unseeded batch cooling crystallization

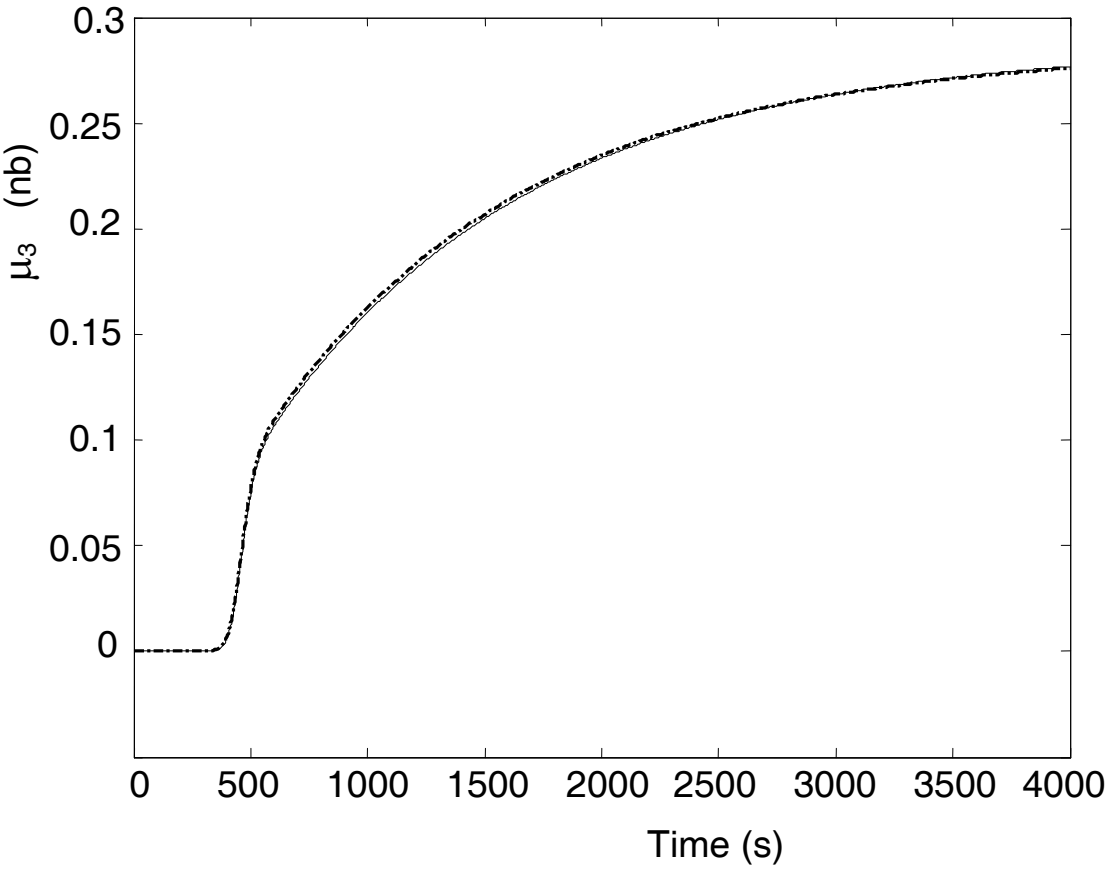

Figure 6: Simulation (solid line) and reconstructed time variations (Dashed line) of the third moment of the size distribution during unseeded batch cooling crystallization

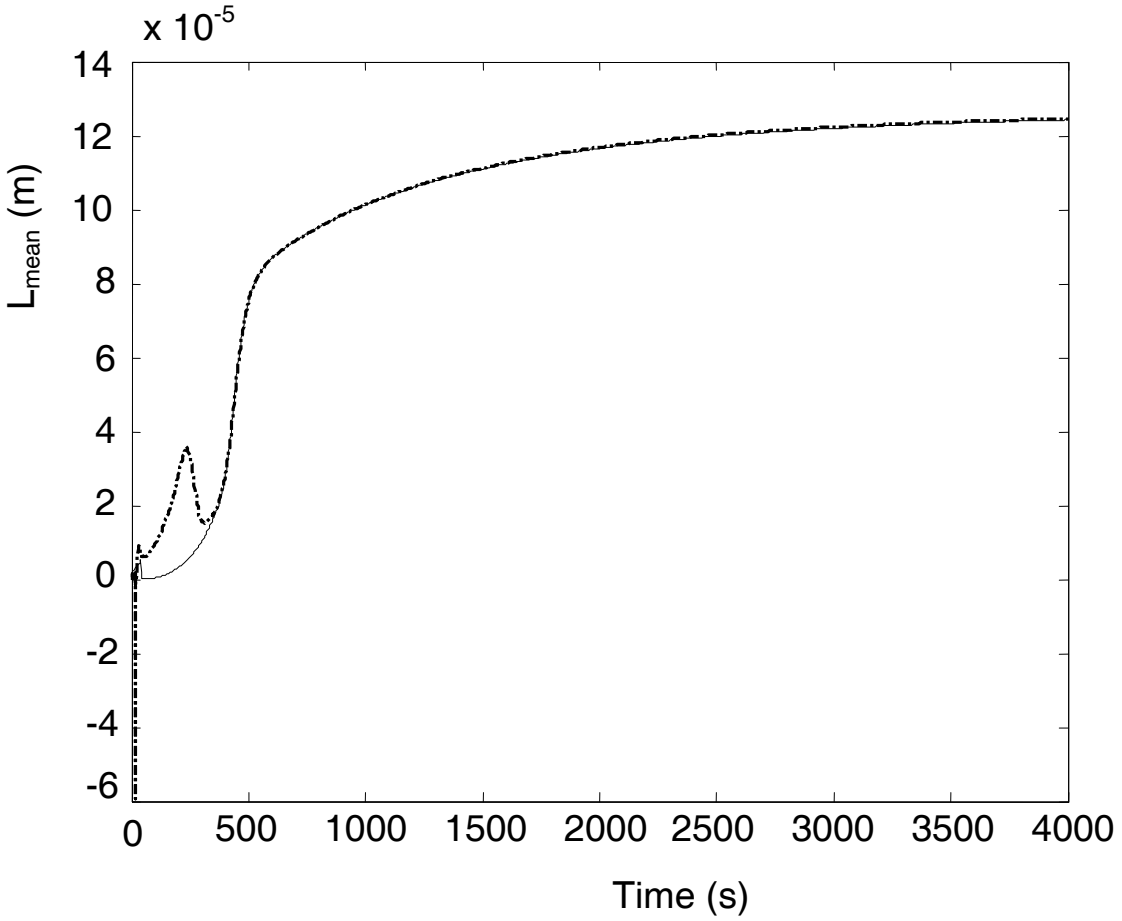

Figure 7: Simulation (solid line) and reconstructed time variations (Dashed line) of the number average particle size during unseeded batch cooling crystallization

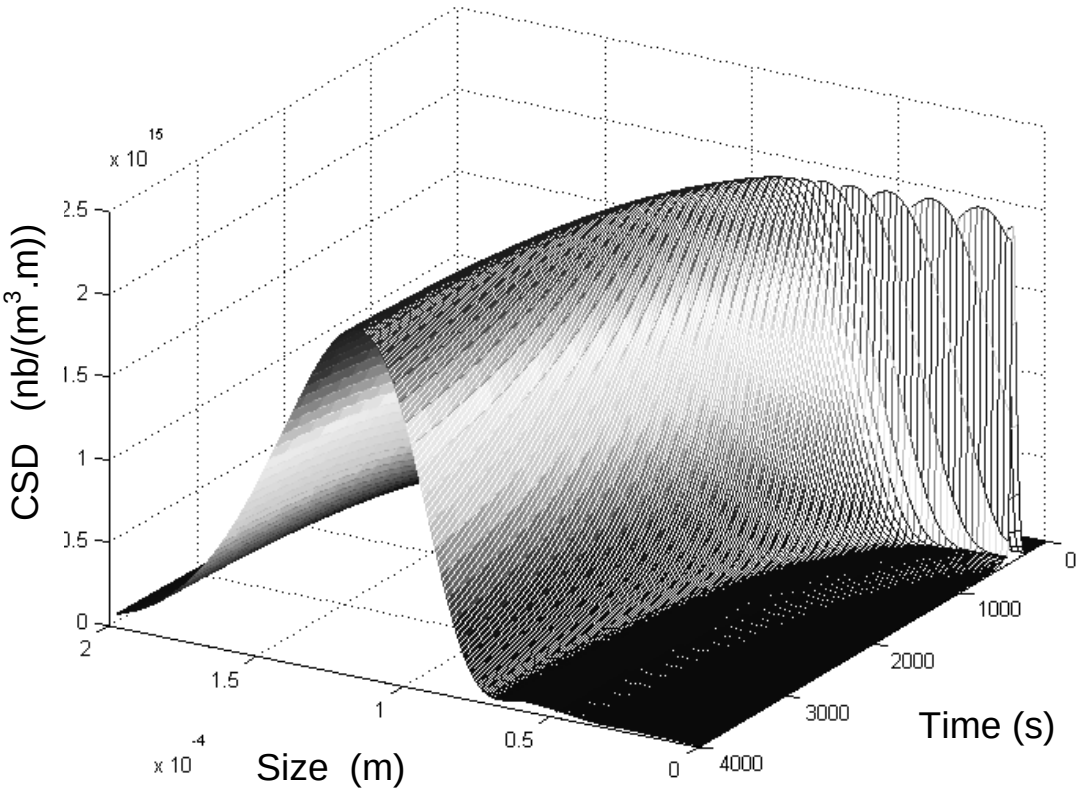

Figure 8: Simulation of the time variations of the CSD during unseeded batch cooling crystallization of adipic acid.

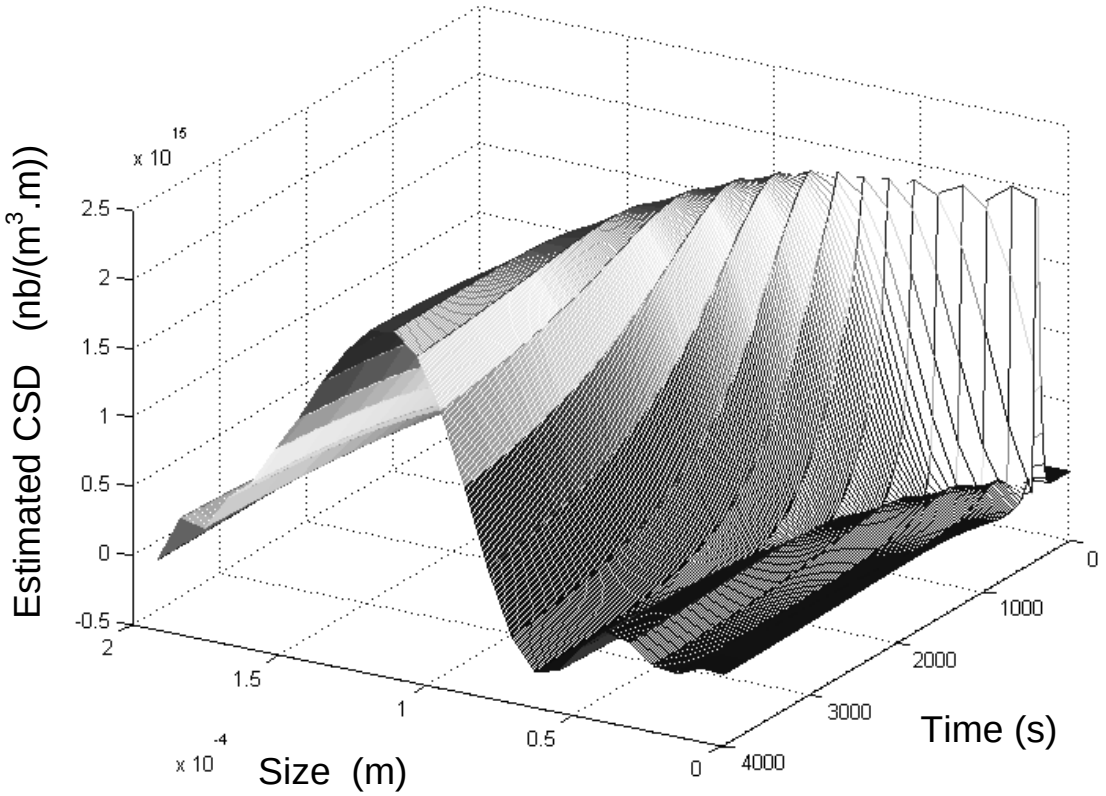

Figure 9: Estimation of the time variations of the CSD during unseeded batch cooling crystallization of adipic acid.

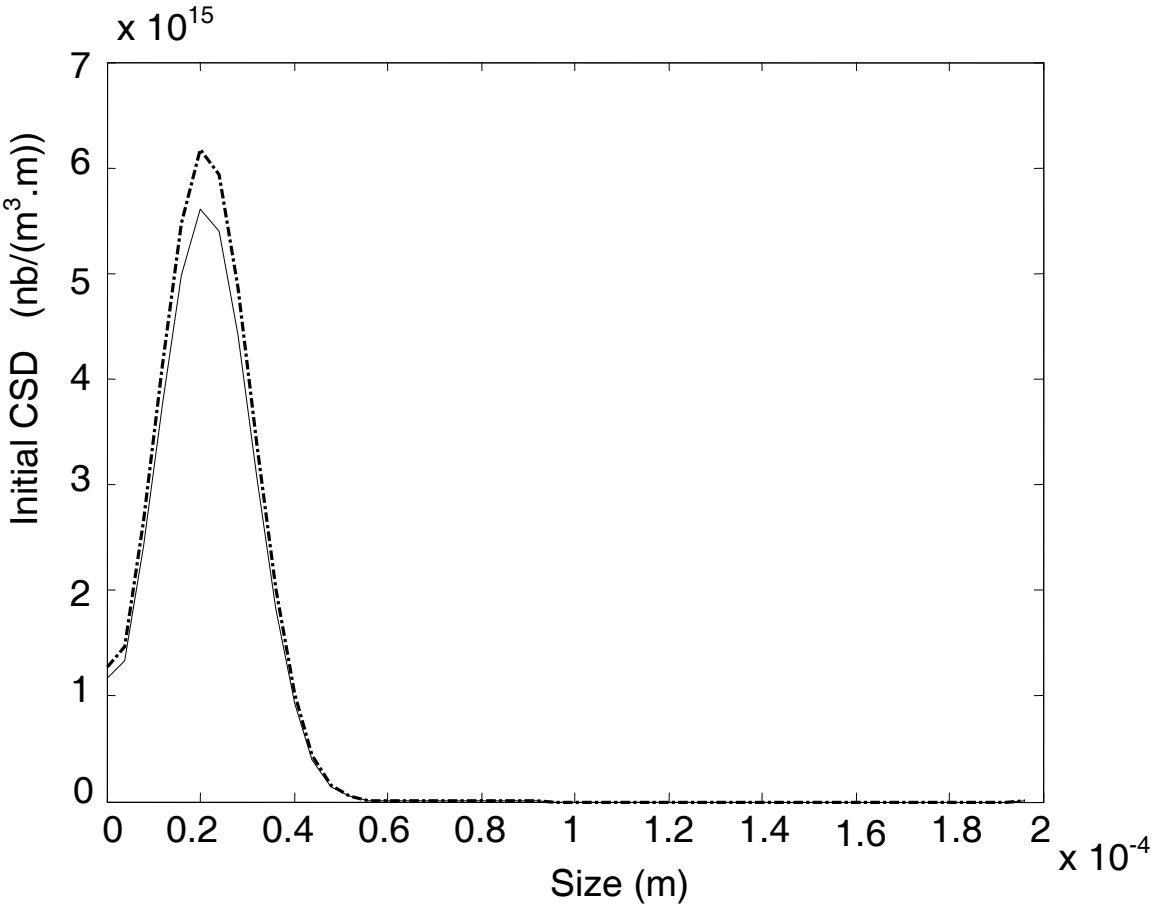

Figure 10: (dashed line) Initial observer CSD (A 10% uncertainty was added to the simulated seed CSD) and (solid line) simulated seed CSD during “case 2” batch cooling crystallization.

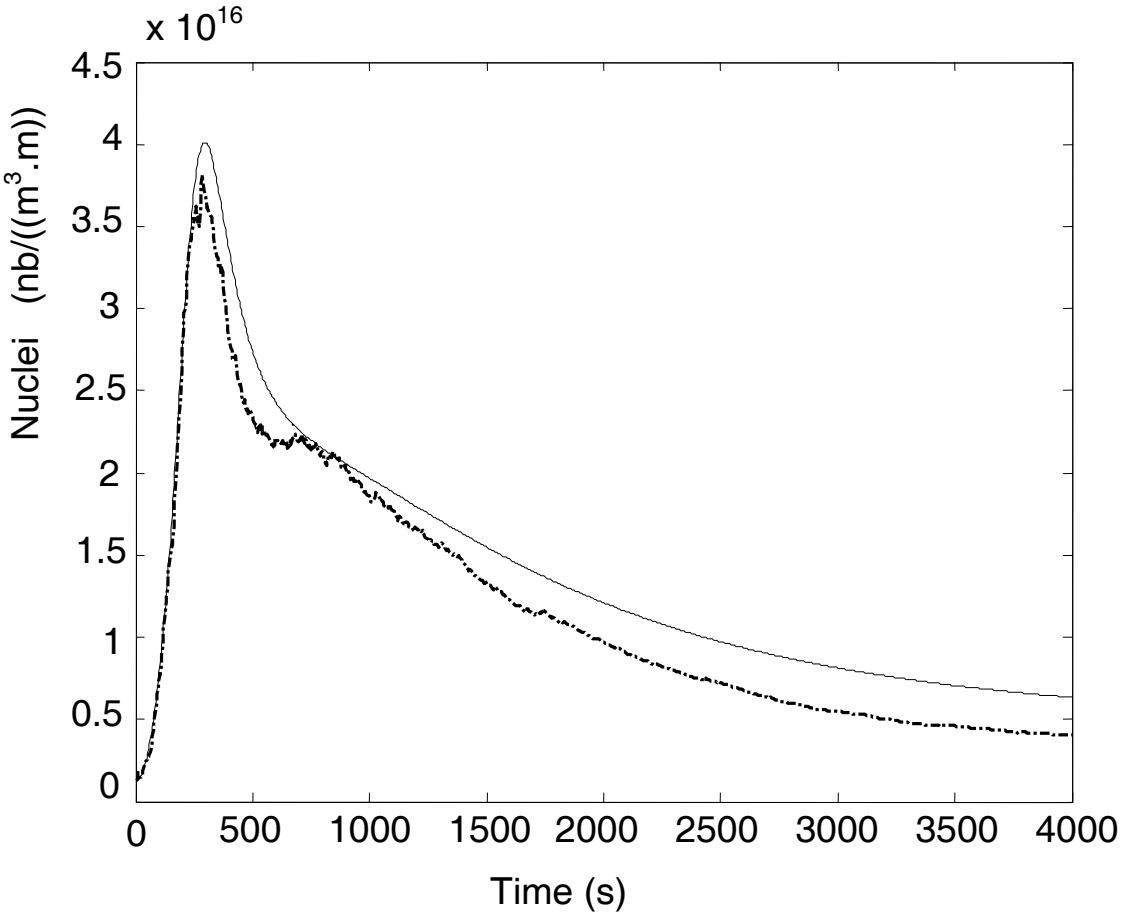

Figure 11: Simulated measurement of the number of nuclei (continuous line) and estimates (Dashed line) during seeded batch cooling crystallization.

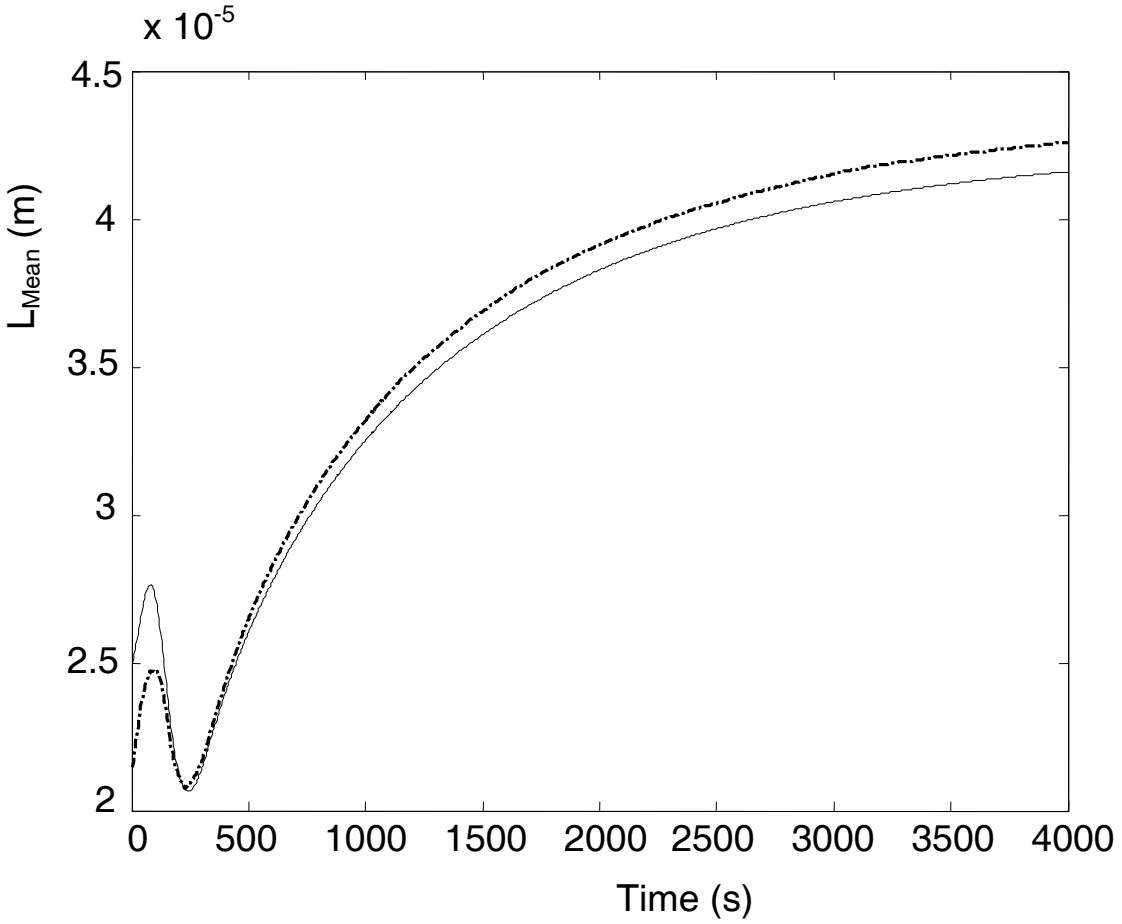

Figure 12: Simulation (solid line) and reconstructed time variations (Dashed line) of the number average particle size during seeded batch cooling crystallization.